Materials Advances

ROYAL SOCIETY OF CHEMISTRY

PAPER

View Article Online
View Journal | View Issue



Cite this: *Mater. Adv.*, 2025, **6**, 6742

# Hyperbranched poly(ethylene glycol)–trimesic acid polyesters as tunable scaffolds for modulating oxidative stress, calcium homeostasis, and neuro–keratinocyte interactions in tissue engineering

Aniruddha Mukherjee,[a] Satish Kumar,[b] Sayan Basak,[c] Luna Goswsmi,[d] Chandan Goswami,[b] Jagannath Chanda,[e] Prasenjit Ghosh,[e] Rabindra Mukhopapdhyay[e] and Abhijit Bandyopadhyay *[f]

The design of bioengineered scaffolds with tunable mechanical and biochemical properties is essential for advancing tissue regeneration strategies. In this study, we developed a series of hyperbranched poly(ethylene glycol)–trimesic acid (PEG : TMA) polyesters as customizable scaffolds for skin tissue engineering and peripheral nerve modulation. By systematically varying the PEG : TMA ratio (1 : 0.5 to 1 : 5), we achieved controlled branching and crosslinking, resulting in scaffolds with modifiable porosity and stiffness. The 1 : 2 PEG : TMA composition (S3) exhibited optimal characteristics—porosity (~0.73 μm) and modulus (2–12 GPa)—to support efficient nutrient diffusion and robust cell adhesion, as evidenced by enhanced mitochondrial membrane potential (MMP) and regulated reactive oxygen species (ROS) levels. In contrast, the more densely crosslinked 1 : 5 formulation (S5) promoted keratinocyte alignment, neuronal adhesion, and neuro–epidermal interactions, while reducing oxidative stress and modulating basal cytosolic $Ca^{2+}$ concentrations. Together, these findings highlight the potential of hyperbranched PEG : TMA scaffolds to finely tune cellular behavior and microenvironmental cues critical for tissue repair. The demonstrated biocompatibility, mechanical versatility, and bioactivity position this material platform as a promising candidate for regenerative medicine applications.

Received 11th March 2025,
Accepted 28th July 2025

DOI: 10.1039/d5ma00216h

rsc.li/materials-advances



## 1. Introduction

Keratinocyte functions are intimately connected to peripheral nerve endings, highlighting the importance of neuro–keratinocyte interactions for maintaining proper skin function. This emphasizes the critical need for advanced biomaterials that can mimic extracellular matrix features, support the growth of both keratinocytes and peripheral neurons, and possibly other cell types also to enhance cellular responses. This concept serves as the primary hypothesis for this investigation. In this study, we attempt to bridge the biological need for neuro–keratinocyte supportive micro-environments with a biomaterial solution, *i.e.* the hyperbranched PEG : TMA polyesters—designed to modulate multiple factors such as oxidative stress, $Ca^{2+}$-signalling, and cell–matrix interactions for specific tissue engineering and reprogramming purposes. Although the hypothesis involves understanding neuro–keratinocytes cross talk, the same or similar hyperbranched PEG : TMA polyesters can also be used as scaffolds for other complex purposes, such as skin repair and muscle regeneration in future. This is plausible as biological systems are mostly regulated by common signalling pathways, including oxidative stress modulation, $Ca^{2+}$-homeostasis, and interaction with the extracellular matrix. Besides the establishment of functional interactions among peripheral neurons and keratinocytes, this work provides a proof-of-principle that such materials can also be used for regenerative medicine targeting other biological systems.

[a] *Department of Microbiology, Gurudas College, University of Calcutta, 1/1, Suren Sarkar Road, Jewish Gaveyard, Phool-Bagan, Narkeldanga, Kolkata 700054, India*
[b] *School of Biological Sciences, National Institute of Science Education and Research, Bhubaneswar, Khurda, Odisha 752050, India*
[c] *Emulsion Division, Product and Application Development Group, Lion Elastomers, Geismar, Louisiana 70734-3526, USA*
[d] *School of Biotechnology and School of Chemical Engineering, KIIT Deemed to be University, Patia, Bhubaneswar, Odisha 751024, India*
[e] *Hari Shankar Singhania Elastomer and Tyre Research Institute, Hebbal Industrial Estate, Hebbal Industrial Area, Mysuru, Karnataka 570016, India*
[f] *Departmemt of Polymer Science and Technology, University of Calcutta, 92, A.P.C Road, Kolkata 700009, India. E-mail: abpoly@caluniv.ac.in, abhijitbandyopadhyay@yahoo.co.in*

So far, researchers have investigated the integration of branching and crosslinking agents into PEG-based systems to improve their mechanical strength, porosity, and bioactivity.[1,2] A promising approach involves the use of trimesic acid (TMA), a trifunctional monomer that promotes hyperbranching in PEG-based polymers.[3] The combination of PEG and TMA yields hyperbranched PEG : TMA polyesters characterized by a high density of functional end groups, a tunable ratio of soluble (branched) to insoluble (crosslinked) components, and an optimized porous architecture.[4–7] These hyperbranched polyesters are highly suitable for tissue regeneration due to their ability to provide substantial mechanical support, enhance cell adhesion, and regulate biochemical signaling.[8,9]

Our research group previously demonstrated the successful synthesis of non-traditional polyesters using low molecular weight PEG ($M_n$ = 4000) and biocompatible TMA through stoichiometric feeding of PEG and TMA in mole ratios ranging from 1 : 0.5 to 1 : 5.[10] The melt condensation process was carried out under catalytic conditions for 6 hours to prevent gelation caused by excessive functional groups. Suitability for bioapplications was validated through surface texture studies and cell cytotoxicity analyses.[10] Scanning electron microscopy performed in this study revealed adequate micro-voids on the polyester surface, while cytotoxicity studies confirmed that these surfaces supported mammalian cell adhesion, growth, and viability, as demonstrated by successful MTT assay results.[10] Building on this foundational knowledge, we aimed to leverage these insights and explore further applications of hyperbranched PEG : TMA polyesters.[11] Recent findings suggest that these materials can influence critical physiological processes such as oxidative stress management, $Ca^{2+}$-homeostasis, and mitochondrial function, which are essential for better cell functions and repair.[12]

In this context, oxidative stress from excess ROS causes cellular aging, mitochondrial dysfunction, and reduced repair ability.[13] Hyperbranched PEG : TMA polyesters effectively reduce intracellular ROS levels and stabilize mitochondrial membrane potential, protecting cells from oxidative damage and apoptosis[14]. Additionally, these polymers modulate $Ca^{2+}$-signaling—a crucial process for cell functions by regulating $Ca^{2+}$-dynamics, signaling, and enhancing cell activation and differentiation.[15]

The mechanical properties of PEG : TMA polyesters mimic the extracellular matrix, offering stability, structural reinforcement, and alignment.[16–20] Their tunable porosity and strength can enhance the cell adhesion, proliferation, migration, and facilitate nutrient transport.[21–25] Furthermore, these scaffolds may support interactions between different and other cell types, thus may turn out to be useful for handling complex biological problems, such as neuromuscular junction repair, angiogenesis, muscle regeneration and other aspects.[26–29]

Interestingly, hyperbranched PEG : TMA polyesters also allow for extensive bioactive functionalization due to their reactive end groups.[30] This enables the incorporation of growth factors, anti-inflammatory agents, and cell-adhesion peptides, delivering targeted signals to promote cell proliferation, differentiation, and ECM remodeling. Stimulus-responsive scaffolds further enable precise, on-demand drug delivery, making them highly adaptable for customized muscle regeneration therapies.[31–33]

This study evaluates hyperbranched PEG : TMA polyesters as regenerative scaffolds for neuro–keratinocyte interaction and functional crosstalk. It examines how these polymers affect ROS production, $Ca^{2+}$-balance, and mitochondrial function in cells by analyzing their mechanical properties, surface morphology, and bioactivity. We anticipate that the findings may also support the development of biomaterials to treat other complex disorders by providing structural support and promoting tissue healing, making PEG : TMA polyesters a promising option for tissue restoration.

## 2. Materials and methods

### 2.1. Raw material for polyester synthesis

PEG with a number average molecular weight of 4000 g $mol^{-1}$ and TMA exhibiting 99.5% purity by weight were utilized as monomers in the synthesis of polyesters. The materials were obtained from Sigma Aldrich Chemical Company, USA, and utilized without additional purification. Concentrated $H_2SO_4$ (36N) served as the catalyst in the synthesis process. The synthesized polymers underwent purification through precipitation from diethyl ether, which served as a non-solvent. Concentrated $H_2SO_4$ and diethyl ether were acquired from local suppliers. Distilled water produced in the laboratory was utilized during the experiments as needed.

### 2.2. Synthesis of polyesters

Polyesters were synthesized using 4000-number PEG and 99.5%-purity TMA, as specified in our previous work. By utilizing regulated stoichiometry, the polyesters were synthesized to achieve maximal solubility, as indicated by the solubility data provided in Table S1.[10] The properties of these polyesters, as observed from our experimental results, are summarized in Table S2.[10]

All feed ratios are expressed in the format PEG : TMA (mol : mol). Thus, a 1 : 0.5 ratio indicates an excess of PEG, while 1 : 5 indicates an excess of TMA, which contributes to increased branching and crosslinking density.

### 2.3. Atomic microscopic measurement

The powdered samples were prepared by dissolving approximately 2 mg of polymer in 1 mL of distilled water (2 mg $mL^{-1}$), followed by drop-casting 20 μL of this solution onto AFM stubs and air-drying at room temperature before imaging. Five distinct sample concentrations, labelled S1, S2, S3, S4, and S5, were examined. AFM imaging indicated that S3 exhibited unique properties relative to the other samples, although the point modulus for all samples varied between 2 and 12 GPa. The analysis utilized a Park Systems NX10 AFM in tapping mode with a silicon tip.

### 2.4. Measurement of reactive oxygen species (ROS), mitochondrial membrane potential ($\Psi_m$), and intracellular calcium ion ($Ca^{2+}$) levels

**2.4.1. Cell culture.** HaCaT and F-11 cells were cultured in DMEM, and F-12 HAM media, respectively, supplemented with 10% fetal bovine serum (Gibco) and 1% antibiotics (Gibco) in a cell culture incubator (5% $CO_2$, 37 °C). For 2D cell culture, polyesters were coated onto glass coverslips, air-dried aseptically, and UV-sterilized for 3 hours.

**2.4.2. Analysis of mitochondrial and intracellular reactive oxygen species.** HaCaT cells were seeded on polyester-coated glass coverslips and cultured for 48 hours at 37 °C in standard cell culture media. To detect mitochondrial and intracellular ROS, cells were washed twice with 1X PBS and then incubated with MitoSOX (2.5 μM, Invitrogen) and H2DCFDA (10 μM, Invitrogen) dyes for 20 minutes in serum-free media at 37 °C. Cells exposed to 20 μM of $H_2O_2$ served as the positive control. ROS signals were detected using a confocal microscope (Olympus FV 3000) with identical imaging parameters (such as laser power, gain, exposure time, and detector settings) applied uniformly across all samples. This standardization ensured that observed fluorescence differences are due to biological variation.

**2.4.3. MMP ($\Psi_m$) analysis.** The mitochondrial membrane potential of cells cultured on various polyester surfaces was assessed using TMRM (tetramethyl rhodamine methyl ester, perchlorate, invitrogen) dye (50 nM, Invitrogen). Fluorescence intensity was observed and recorded using confocal microscopy. MMP analysis was detected using a confocal microscope (Olympus FV 3000) with identical imaging parameters—laser power, gain, exposure time, and detector settings—applied uniformly across all samples. This standardization ensured that observed fluorescence differences reflected biological variation mainly.

**2.4.4. $Ca^{2+}$-imaging.** Intracellular $Ca^{2+}$-levels in cells cultured on different polyester surfaces were measured using Fluo-4-AM dye at a concentration of 1 μM for 30 minutes (Invitrogen). $Ca^{2+}$-imaging was detected using a confocal microscope (Olympus FV 3000) with identical imaging parameters (such as laser power, gain, exposure time, and detector settings) applied uniformly across all samples. This standardization ensured that observed fluorescence differences reflected biological variation mainly.

### 2.5. Co-culture of F-11 and HaCaT Cells

HaCaT cells and F-11 cells were co-cultured in a 1 : 1 ratio on different hydrogel surfaces for 24 hours under standard cell culture conditions. Afterward, the cells were washed with 1× PBS and fixed for 15 minutes at room temperature using a 2% paraformaldehyde solution (PFA). F-11 cells were immunodetected using a β-III tubulin antibody (1 : 500, Sigma-Aldrich). Phalloidin coupled to Alexa Fluor 594 (1 : 500, Invitrogen) was used to stain the actin filaments of both cell types. Nuclei were counterstained with DAPI and mounted on a glass slide. Images were observed under a confocal microscope and quantified using ImageJ.

**2.5.1. Statistical tests.** All statistical analyses were performed using GraphPad Prism 9. Data are expressed as mean ± standard deviation (SD). One-way ANOVA followed by Tukey's *post hoc* test was used to assess significance across multiple groups. A $p$-value of $<0.05$ was considered statistically significant unless otherwise stated. Sample sizes ($n \geq 100$ cells per group) were maintained for most of the quantifications.

## 3. Result and discussion

### 3.1. Synthesis and solubility of the polyesters

The polyesters were synthesized using PEG with a molecular weight of 4000 g $mol^{-1}$ and TMA as a trifunctional monomer. PEG, due to its polyfunctional nature, has a propensity to gel early in the polymerization process.[33–35] This gelation is a significant challenge, as it can limit the extent of polymerization and affect the physical properties of the final product. To address this, the mole composition of TMA was carefully controlled, ranging from lower to slightly higher concentrations, in order to optimize the development of branching while delaying gelation (Table S1).[36] Branching occurs early in the process, before gelation, and thus the judicious selection of TMA concentrations was crucial for maintaining a balance between branching and gelation, ensuring the formation of soluble, high-quality polyesters.[37] Detailed $^1$H NMR analyses confirming branching percentage, terminal group conversion, and degree of esterification for PEG : TMA compositions synthesized using the same ratiometric method were previously reported by our group.[38] These findings underpin the structural interpretations discussed here.

The reactions were conducted for a fixed period of 6 hours, which is an important factor in controlling the polymerization process.[34] By limiting the reaction time, we effectively mitigated extensive gelation that could otherwise occur due to the overproduction of functional groups.[39] This controlled reaction period allowed the system to produce polyesters with an increased soluble fraction, which is advantageous for their intended use in tissue engineering.[2] The solubility data presented in Table S1 clearly demonstrate that the approach taken was effective, resulting in a significant increase in the quantity of soluble polyesters across all feed compositions, with the solubility values decreasing gradually as the concentration of TMA increased.[40,41]

The synthesis involved both crosslinking (leading to the insoluble fraction) and branching (which contributed to the soluble fraction). The TMA monomer, as a trifunctional molecule, served as a nodal point for both processes. The higher the concentration of TMA in the feed, the more prominent the crosslinking, leading to a greater proportion of insoluble material in the final polymer. Conversely, lower concentrations of TMA resulted in polyesters that were more branched but less crosslinked, which led to a higher soluble fraction and a more flexible polymer structure.[33]

Table S1 provides a clear relationship between TMA concentration and the resulting polyester structure. For instance, the polyesters produced at lower TMA concentrations (*e.g.*, S1 and S2, with PEG : TMA ratios of 1 : 0.5 and 1 : 1, respectively) exhibit

higher solubility (90% and 85%) and greater soluble yields (78% and 81%), indicating that these polyesters are more branched and less crosslinked. In contrast, polyesters synthesized at higher TMA concentrations (*e.g.*, S3, S4, and S5, with PEG : TMA ratios of 1 : 2, 1 : 3, and 1 : 5, respectively) show decreasing solubility (78%, 70%, and 62%) and lower soluble yields (64.7%, 60.2%, and 54.5%), reflecting a shift towards a more hyperbranched structure with greater crosslinking. The presence of trifunctional TMA at higher concentrations promotes more crosslinking, which reduces the overall solubility of the polymer while increasing the insoluble portion.

Additionally, the solubility and yield data are consistent with the expected outcomes of branching and crosslinking. As the TMA concentration increases, the polyesters transition from more branched topologies (with higher solubility) to more crosslinked, hyperbranched structures (with lower solubility). Thus, increasing TMA concentration shifts polyesters from branched, highly soluble structures to crosslinked, hyperbranched, less soluble ones, impacting their molecular structure, solubility, mechanical strength, and bioapplication suitability.[42,43] While hyperbranched polymers are generally more soluble than their linear analogues due to their globular, less entangled architecture, the observed decrease in solubility at higher TMA concentrations in our system is not indicative of pure hyperbranching. Rather, it reflects a transition toward increased crosslinking density. As the molar ratio of TMA rises (*e.g.*, in S5), the trifunctional nodes promote extensive intermolecular bonding beyond the gelation threshold, leading to the formation of an increasingly rigid, insoluble network. Although branching continues to increase, the formation of insoluble crosslinked domains becomes dominant, thereby reducing overall solubility. This behaviour confirms that the system changes from a primarily hyperbranched topology to a hybrid structure where crosslinking predominates.[29]

To clarify, while hyperbranched polymers are generally soluble due to their non-crosslinked, dendritic architecture, the observed decrease in solubility at higher TMA concentrations in our study reflects the dominance of crosslinking over pure branching. As TMA concentration increases, trifunctional nodes promote network formation beyond the gelation threshold, resulting in denser, insoluble structures. Thus, the solubility reduction from S3 to S5 is primarily due to increased crosslinking density, not hyperbranching alone.

These polyesters with different branching and crosslinking characteristics are particularly relevant for tissue engineering applications, where the balance between solubility, mechanical strength, and bioactivity is critical. The hyperbranched structures, which occur at higher TMA concentrations, can provide increased mechanical stability and support for cell attachment and growth, making them suitable as scaffolds.[11,16,17] Although the structural interpretation of S3 is supported by solubility, porosity, and surface morphology, this remains a qualitative assessment. In our previous work,[38] PEG : TMA polyesters were characterized with respect to $^1$H NMR end-group integration to calculate branching indices, thereby confirming the architectural transitions as a function of feed ratio. While this evidence supports the present interpretation, future work will focus on direct quantification within this series to enhance these claims further. A more detailed structural characterization of similarly synthesized PEG : TMA-based hyperbranched systems, including NMR-based branching index analysis and solubility correlation, is available in our previous study[6,7,43,44] These results provide complementary support for the architecture proposed here. On the other hand, the more branched polyesters, which exhibit higher solubility, may offer more flexibility and a better environment for cell proliferation and migration, which are key factors in tissue healing.[43,44]

### 3.2. Analysis of AFM of different polyesters

AFM analysis (Fig. 1) provides insights into the surface morphology and mechanical properties of PEG : TMA polymer compositions synthesized at different stoichiometric ratios (1 : 0.5, 1 : 1, 1 : 2, 1 : 3, and 1 : 5). Additional structural characterization using SEM and FT-IR for similarly synthesized PEG : TMA scaffolds has been reported previously by our group,[45] confirming microvoid porosity and ester bond formation, respectively. Furthermore, fluorescence/confocal images presented in this study (Fig. 2–5) show scaffold–cell interactions, supporting the material's structural suitability for biological applications. All samples demonstrated a modulus range of 2–12 GPa under dry, ambient AFM conditions. However, PEG-based scaffolds—including PEG : TMA—are known to soften substantially under hydrated conditions, often exhibiting modulus values in the low MPa to kPa range depending on crosslinking density. The formulations used in this study for biological testing were synthesized with reduced crosslinking to ensure mechanical compliance suitable for skin and neuronal tissue applications.[46,47] It is important to note that these values characterize the surface stiffness measured with AFM under ambient (dry) conditions. These do not represent any sort of bulk modulus of hydrated scaffolds, which is believed to be far lower and approaching the realm of soft tissues like skin and muscle. While the AFM-measured modulus range (2–12 GPa) is an indication of mechanical strength at the surface level, it does not directly inform one of bulk biocompatibility. Biocompatibility is assumed to provide a fine balancing act between surface stiffness, porosity, and molecular architecture, which become evident in the formulation of S3. The observed variations in surface morphology and mechanical response can be directly attributed to the differences in the branching and crosslinking behaviors, which have been thoroughly characterized by complementary spectroscopic, SEM, and biocompatibility analyses. Although SEM data are not presented in this study, similar PEG : TMA polyester scaffolds were extensively characterized by scanning electron microscopy in our previous publication.[38] In that work, we observed a trend of decreasing porosity and increased surface compactness with higher TMA content, which is consistent with the AFM findings reported here. These prior observations further support the progressive crosslinking and morphological densification inferred from the current analysis.

The 1 : 2 PEG : TMA ratio (S3) exhibited a significantly different surface morphology, demonstrating the optimal equilibrium

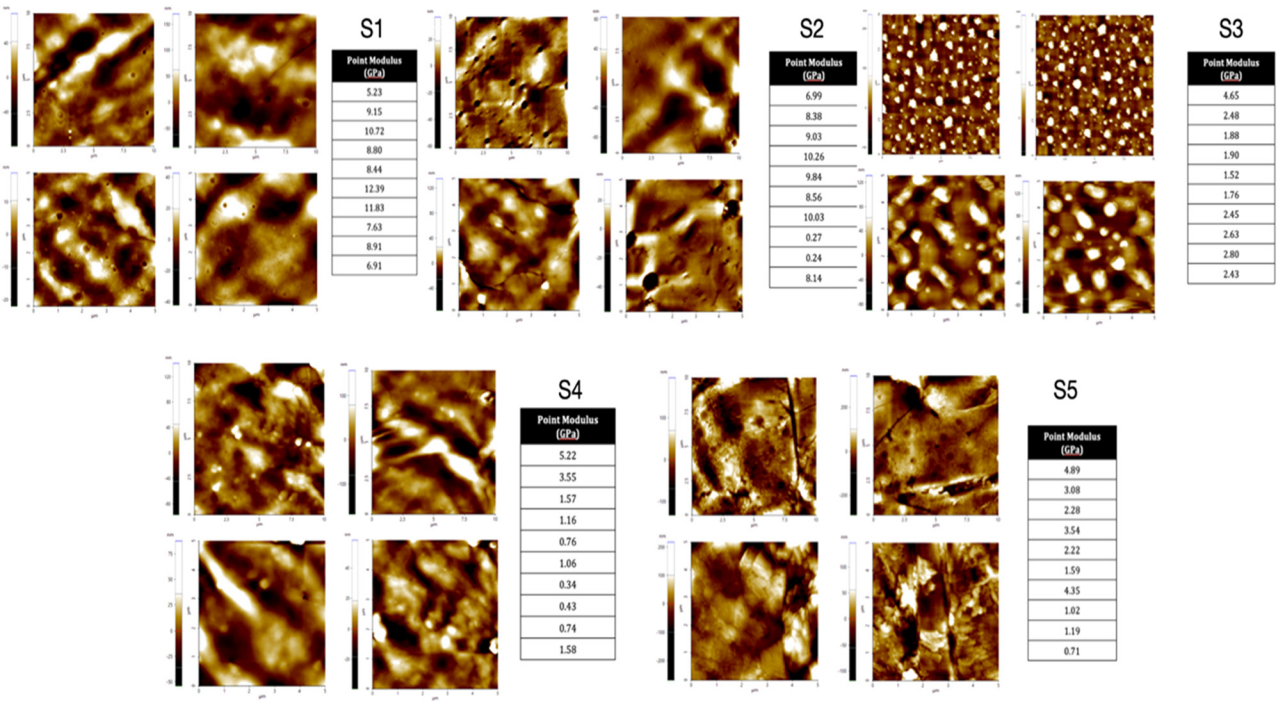


Fig. 1 Atomic force microscopic analysis of different polyesters (S1–S5).

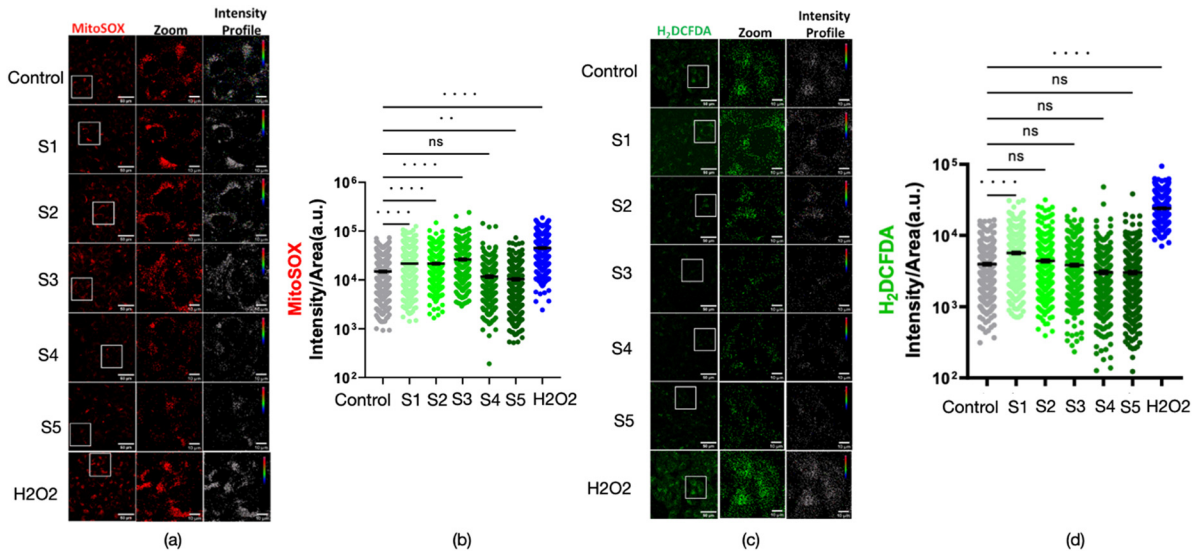


Fig. 2 Mitochondrial ROS levels in HaCaT cells cultured on different hydrogel surfaces were assessed. (a) Cells were treated with MitoSOX dye for 24 hours, and confocal images (left column) showed mitochondrial ROS levels. Enlarged images (middle column) demonstrate ROS distribution, with fluorescence intensity profiles represented in pseudo-rainbow color (red for high, blue for low ROS) in the right column. (b) Fluorescence intensity from ≥100 cells per condition is quantified. Statistical significance: **** = $P < 0.0001$, ** = $P < 0.01$, ns = non-significant (one-way ANOVA). (c) ROS levels in HaCaT cells on glass (control) or on hydrogel surfaces were analyzed. Representative confocal images (right column) and intensity profiles (pseudo-color scale) show ROS distribution. (d) Quantification of fluorescence intensity ($n \geq 100$ cells) per condition. Statistical significance: **** = $P < 0.0001$, ns = non-significant, determined by one-way ANOVA.

between branching and crosslinking. This was confirmed by FTIR, UV, and $^1$H NMR analyses, which revealed a substantial degree of ester bond formation and TMA capping. SEM analysis corroborated these findings, showing that S3 had microvoids (~0.73 μm) embedded within a cohesive matrix, providing enhanced porosity that would facilitate nutrient diffusion and improve cell adhesion.[33] The AFM data further support these observations, indicating that the surface of S3 is highly favorable for bioapplications, including tissue engineering. The microstructural features of S3 align with the ideal requirements for

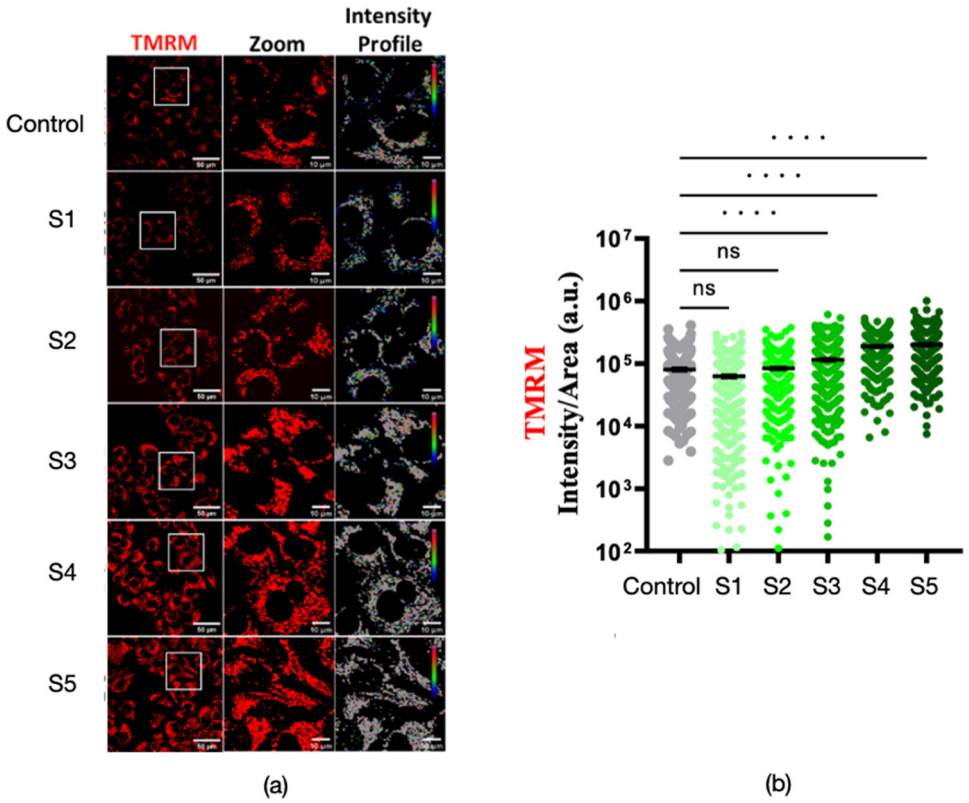


Fig. 3 Hydrogel surfaces influence the mitochondrial membrane potential ($\Delta\Psi_m$) of HaCaT cells. HaCaT cells were cultured on various hydrogel surfaces for 24 hours, stained with TMRM dye (which accumulates in active mitochondria), and analyzed using live-cell confocal microscopy. (a) Representative confocal TMRM fluorescence images of HaCaT cells are shown (left panel). Enlarged views of selected regions (white boxes) are presented in the middle column, while pseudo-colored intensity profiles of TMRM fluorescence (red = higher $\Delta\Psi_m$, blue = lower $\Delta\Psi_m$) are displayed in the right column. (b) Fluorescence intensity was quantified for ≥100 cells per condition using ImageJ. ****$P < 0.0001$; ns = not significant (one-way ANOVA).

cellular interactions, which are essential for regenerative processes. Its porosity allows for efficient mass transport, while its mechanical properties maintain integrity under physiological conditions, suggesting its suitability for long-term implantation.

In contrast, the 1 : 0.5 (S1) and 1 : 1 (S2) sample, characterized by predominantly branched structures with minimal crosslinking, exhibited smoother and less differentiated surface morphologies. These samples showed higher solubility and lower density, consistent with the limited crosslinking observed in previous analyses.[48,49] While the high solubility of S1 and S2 is advantageous for certain applications, such as those requiring biodegradability or rapid dissolution, their lack of crosslinking severely compromises their mechanical stability.[50] This smooth surface structure is suboptimal for cellular adhesion, as the lack of distinct topographical features limits the engagement of cells with the polymer, reducing the likelihood of successful tissue integration.[46] Consequently, while these materials may be appropriate for short-term applications where solubility is prioritized, they fall short in applications requiring sustained mechanical strength and cellular interactions.

On the other hand, the 1 : 3 (S4) and 1 : 5 (S5) samples, characterized by excessive crosslinking, exhibited denser, more homogeneous surface structures with markedly reduced porosity. These samples demonstrated a tighter, more rigid network, as revealed by both AFM and SEM imaging, which correlates with the lower solubility observed in the corresponding data. However, this increase in crosslinking leads to a significant reduction in the polymer's ability to support cellular adhesion and migration. The decreased surface roughness and porosity impede the necessary interactions between the scaffold and the cells, diminishing the material's ability to promote tissue regeneration.[45,47] Although these highly crosslinked structures provide enhanced mechanical strength, they compromise cell accessibility and nutrient exchange, rendering them less suitable for applications requiring dynamic cellular engagement and tissue remodeling.[36]

### 3.3. Determination of reactive oxygen species (ROS), mitochondrial membrane potential ($\Psi_m$), and intracellular calcium ion ($Ca^{2+}$) levels

A study of ROS production in HaCaT cells grown on polyester substrates (S1–S5) explores the relationship between surface morphology, molecular structure, and cellular oxidative stress.[45] Confocal imaging (Fig. 2) using MitoSOX and H2DCFDA dyes

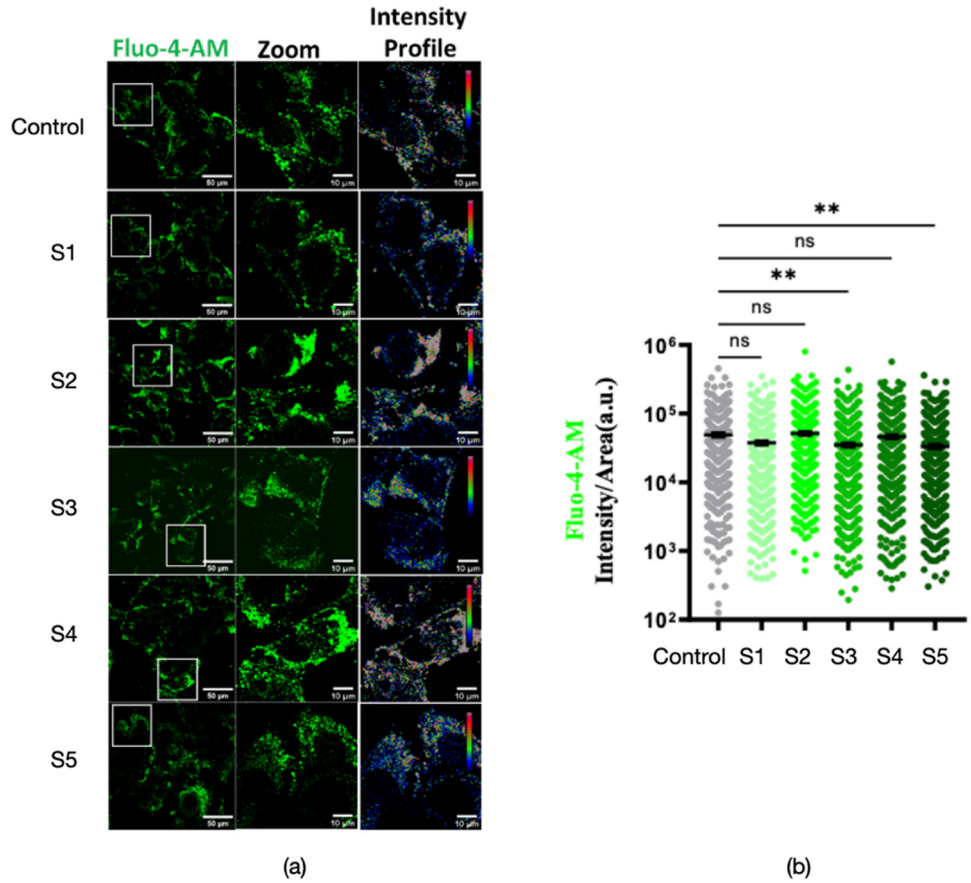


Fig. 4 Intracellular $Ca^{2+}$-levels in HaCaT cells were analyzed after 24 hours of culture on various hydrogel surfaces (1–0.5, 1–1, 1–2, 1–3, and 1–5). Cells were labeled with Fluo-4 AM dye, and changes in intracellular $Ca^{2+}$ were visualized *via* live-cell confocal imaging. (a) Representative confocal images of HaCaT cells on different surfaces are shown (left column). Zoomed-in images (middle column) highlight regions of interest, showing $Ca^{2+}$ variations. Fluorescence intensity profiles of Fluo-4 AM in these regions (white boxes) are displayed in pseudo-color, with red indicating highest and blue lowest $Ca^{2+}$-levels. (b) Fluo-4 AM fluorescence intensity per cell was quantified ($n \geq 100$ cells per condition) using ImageJ and presented as a bar graph. $^{**}P < 0.01$; ns = not significant (one-way ANOVA).

revealed distinct effects of these surfaces on mitochondrial and cellular ROS levels.

Cells on S1 (1 : 0.5 PEG : TMA) exhibited significantly higher ROS levels compared to the control and other polyester surfaces. This correlates with AFM findings, which indicated a smoother surface for S1, potentially impairing cell adhesion and promoting stress signaling.[51] NMR analysis confirmed minimal branching (26%) in S1, limiting the formation of an optimal microenvironment, and thus contributing to oxidative stress. Despite elevated mitochondrial ROS levels, these were lower than in S3, suggesting surface properties and molecular structure influence stress responses (Fig. 2).

S3 (1 : 2 PEG : TMA), with optimal branching (55%) and moderate crosslinking, induced the highest mitochondrial ROS levels, aligning with its AFM and NMR characterization. These features facilitate adequate cell adhesion and provide functional end groups, triggering stress signaling pathways and increased mitochondrial oxidative stress.[52] This may suggest that the porous surface of an S3 sample ($\sim$0.73 μm) may help attenuate cellular oxidative stress in the presence of elevated mitochondrial ROS levels. Surface roughness and porosity may play an important role in mediating cellular stress response by either enhancing cell–material interactions or by facilitating the diffusion of oxygen or nutrients; however, the mechanistic details remain unclear. Further investigation is needed to identify whether oxidative modulation is primarily governed by integrin-mediated adhesion signaling, changes in mitochondrial dynamics, or by mass transport improvement. However, cellular ROS levels in S3 were comparable to the control, indicating that its surface porosity ($\sim$0.73 μm) and structural coherence helped mitigate widespread cellular stress despite mitochondrial hyperactivation (Fig. 2).[52] Although S3 exhibited elevated mitochondrial ROS levels, cellular ROS remained comparable to the control, suggesting a degree of oxidative containment. However, the long-term consequences of mitochondrial hyperactivity were not assessed in this study, and further analysis of apoptosis, viability, and sustained redox balance will be necessary to confirm S3's suitability for extended use.

On the other hand, S5 (1 : 5 PEG : TMA), with its hyperbranched structure and extensive crosslinking, exhibited the lowest mitochondrial and cellular ROS levels, suggesting its

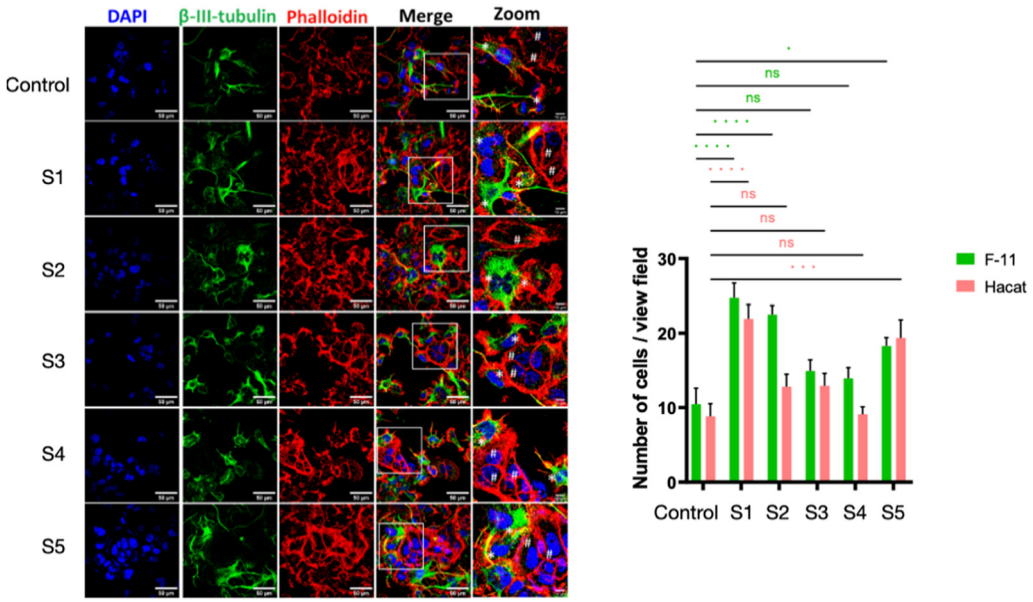


Fig. 5 Differential support of hydrogel surfaces for co-culture. F-11 (peripheral neuronal) and HaCaT (keratinocyte) cells were grown at a 1 : 1 ratio for 24 hours. Representative confocal images display F-11 cells (green fluorescence, labelled by ß-III tubulin), with cellular morphology visualized by Phalloidin (red fluorescence, actin filaments) and DAPI (blue fluorescence, nucleus). Cell counts on each surface were obtained using ImageJ ($n \geq 10$ view fields). F-11 and HaCaT cells are marked by * and # in images. Statistical significance: $P < 0.01$, **** = $P < 0.001$, **** = $P < 0.0001$, ns = non-significant, with one-way ANOVA performed. Green ( ) and red (*) asterisks indicate analysis between F-11 and HaCaT cells under each condition.

ability to reduce oxidative stress. AFM and SEM analysis revealed a dense, homogeneous surface with no porosity, while NMR confirmed significant TMA-capping. These structural characteristics likely minimize excessive cell–surface interactions, preventing over-activation of stress signaling pathways.[51] Similarly, S4 (1 : 3 PEG : TMA) maintained ROS levels similar to the control due to its balanced structure and moderate surface cohesion, demonstrating a more stable cellular environment (Fig. 2).

The mitochondrial membrane potential (MMP) analysis (Fig. 3) of HaCaT cells cultured on polyester surfaces (S1–S5) reveals critical insights into how surface architecture and molecular composition influence mitochondrial function.

Polyesters S1 (1 : 0.5 PEG : TMA) and S2 (1 : 1 PEG : TMA) exhibited negligible changes in MMP compared to the control (glass surface). These findings align with AFM and SEM data, which revealed smoother, less porous morphologies in these polyesters. Furthermore, NMR analysis indicated low branching in S1 (26%) and moderate branching in S2, with minimal functional group availability.[33] The smooth surfaces of S1 and S2 likely limited cell adhesion and interaction, resulting in suboptimal conditions for mitochondrial activation and minimal impact on MMP. Polyester S3 (1 : 2 PEG : TMA) demonstrated the most significant increase in MMP among all compositions. This result is consistent with its balanced surface architecture, as observed in AFM and SEM studies, which revealed porosity (~0.73 μm) and moderate crosslinking. NMR analysis further confirmed the highest branching percentage (55%), with sufficient functional end groups to facilitate strong cell–surface interactions. These properties likely created a microenvironment that supported enhanced mitochondrial activity. This is further corroborated by S3's previously reported ability to elevate mitochondrial ROS levels while maintaining cellular ROS levels near control conditions.

Polyesters S4 (1 : 3 PEG : TMA) and S5 (1 : 5 PEG : TMA) also induced elevated MMP levels compared to the control, indicating enhanced mitochondrial function. However, S5, with its hyperbranched and densely crosslinked structure, exhibited similar TMRM intensity to S4, despite its more compact and homogeneous surface morphology, as demonstrated by AFM and SEM data. Interestingly, the high MMP observed in S5 did not correspond to elevated ROS levels, whereas S3 exhibited increased mitochondrial ROS despite a similarly elevated MMP. This suggests that ROS generation in S3 may be driven by enhanced mitochondrial metabolism or external signalling activation, rather than mitochondrial dysfunction. Although MitoSOX and H2DCFDA provide insight into ROS compartmentalization, the study did not distinguish between mitochondrial and NADPH oxidase-derived ROS, warranting further investigation into the specific sources of oxidative stress. The reduced porosity of S5 likely restricted nutrient diffusion and cell–surface interactions, potentially limiting further mitochondrial activation.[52,53] This suggests that excessive crosslinking in S5, while beneficial for reducing ROS and enhancing mechanical integrity, may impose structural constraints that counterbalance mitochondrial activation.

Nevertheless, while smoother surfaces like those of S1 and S2 fail to stimulate significant mitochondrial activity, more structured and balanced surfaces, such as S3, support enhanced MMP by promoting better cell adhesion and

interaction. S4 and S5, with their higher crosslinking levels, still enhance MMP but may reach a plateau in mitochondrial activation due to restricted porosity in S5.

This analysis was conducted in HaCaT keratinocytes to investigate scaffold influence on basal intracellular calcium homeostasis, and not to assess neuronal calcium propagation or excitability, which was beyond the scope of this study (Fig. 4). Confocal imaging with $Ca^{2+}$-sensitive dyes revealed reduced intracellular $Ca^{2+}$-levels across all polyester substrates compared to the control (glass). Here we measured the basal $Ca^{2+}$ for HaCat cells using Fluo4 (a non-ratiometric dye) as a $Ca^{2+}$-sensor. Therefore, the changes observed can be significant in terms of biological functions, but the exact concentration of cytosolic $Ca^{2+}$ measured cannot be commented.

Polyesters S1 (1 : 0.5 PEG : TMA) and S2 (1 : 1 PEG : TMA) exhibited statistically insignificant reductions in intracellular $Ca^{2+}$-levels relative to the control. This aligns with their relatively smoother surface morphologies as observed in AFM and SEM analyses, as well as lower branching percentages (26% for S1 and 40% for S2, based on NMR data). These properties suggest limited mechanotransduction or surface–cell interaction sufficient to influence $Ca^{2+}$-signaling pathways. The minimal functional end groups available in these compositions are likely to further reduce their capacity to alter intracellular signaling. Polyester S3 (1 : 2 PEG : TMA) demonstrated a balanced response, with intracellular $Ca^{2+}$ levels not significantly different from the control. This result complemented previous findings that S3 supports cellular adhesion, mitochondrial activation, and oxidative balance without inducing excessive stress. AFM and SEM analyses revealed a moderately porous surface ($\sim$0.73 μm), with branching and crosslinking (55% branching per NMR) optimized for cell interactions. These features likely provide sufficient mechanical cues to maintain normal $Ca^{2+}$-dynamics, creating a stable microenvironment for cellular signaling.

Polyesters S4 (1 : 3 PEG : TMA) and S5 (1 : 5 PEG : TMA) caused marked reductions in intracellular $Ca^{2+}$ levels compared to the control.[35] S5, in particular, exhibited the most significant decline, consistent with its dense, hyperbranched structure and extensive crosslinking as revealed by AFM, SEM, and NMR analyses. The tightly packed, non-porous surface of S5 restricts cell–surface interactions and impedes effective mechanotransduction, limiting $Ca^{2+}$-influx.

Although S5 lacks surface porosity, its densely crosslinked architecture presents a high density of terminal carboxyl groups from TMA units. These functional groups may enhance cell–material interactions *via* electrostatic and biochemical signalling, thereby facilitating neurite anchorage and extension despite the restricted diffusion environment. This suggests that chemical functionality may partly offset the limitations of low physical porosity. The significant reductions in intracellular $Ca^{2+}$-levels observed for S4 and S5 may be due to reduced mechanotransduction, possibly resulting from the limited porosity and high crosslinking of these surfaces. However, the present study did not investigate specific biochemical pathways such as TRP channel activation or integrin-mediated signalling, which would be necessary to directly validate this mechanism. Additionally, the reduced availability of functional end groups on S5 may further impair pathways essential for $Ca^{2+}$-homeostasis.

Interestingly, S4's effect on $Ca^{2+}$-regulation was intermediate, likely due to its balance of crosslinking and porosity. While S4 supports sufficient adhesion and mitochondrial activity, its increased branching compared to S3 may introduce slight disruptions to $Ca^{2+}$-signaling pathways.

Despite its branching and crosslinking features, S3 did not significantly alter intracellular $Ca^{2+}$-levels, suggesting that its optimized surface morphology preserves cellular signaling pathways. The balanced porosity and mechanical properties of S3 allow effective cell adhesion and signaling without inducing excessive or inhibitory stress. This contrasts with S5, in which excessive crosslinking creates a mechanically restrictive environment, and S1/S2, which lack sufficient functional interaction sites to influence $Ca^{2+}$-regulation.

### 3.4. Differential support of F-11 neuronal and HaCaT keratinocyte cells on polyester surfaces during co-culture

The evaluation of polyester surfaces (S1–S5) for promoting neuro–keratinocyte interactions and enabling co-culture of HaCaT (keratinocytes) and F-11 (neuronal) cells highlights their potential as biomaterials for neuro–keratinocyte tissue engineering. These results collectively indicate (Fig. 5) that PEG : TMA scaffolds support spatial adhesion and coexistence of keratinocytes and neurons. Notably, distinct differences in cellular behavior across the compositions highlight the critical impact of surface properties, as analyzed through AFM, SEM, and NMR, in determining their performance.[33]

Polyester S5 (1 : 5 PEG : TMA) exhibited the most favourable characteristics for co-culture, facilitating robust adhesion of both HaCaT and F-11 cells. Notably, S5 supports direct neurite extensions across keratinocyte islets, enabling efficient neuro–keratinocyte interactions. AFM and SEM analyses revealed that S5 has a dense, homogeneous surface, characterized by hyperbranched (65% as per NMR) and extensively crosslinked architecture, providing a mechanically stable and functional substrate. The low porosity and ample functional end groups, resulting from significant TMA capping, enhance cell attachment and intercellular communication.

Biochemical assays corroborate the superior performance of S5. ROS data indicate minimal oxidative stress, with S5 demonstrating the lowest levels of both cellular and mitochondrial ROS among all surfaces. This reduced oxidative burden creates an environment conducive to prolonged cell survival and interaction. Moreover, TMRM labelling demonstrated that S5 exhibits the highest mitochondrial membrane potential (MMP), signifying enhanced mitochondrial function critical for neuronal expansion, neurite outgrowth, and keratinocyte activity. These findings collectively highlight S5 as the most effective polyester composition for promoting neuro–keratinocyte co-culture and interaction.

Polyester S3 (1 : 2 PEG : TMA) also exhibited favourable properties for neuro–keratinocyte interactions. Its moderately

 

porous surface (~0.73 μm as per SEM), balanced branching (55% per NMR), and crosslinking facilitated significant keratinocyte growth and neurite outgrowth. However, S3 demonstrated slightly elevated mitochondrial ROS levels, suggesting that its architecture may induce marginal oxidative stress. While S3 supports strong initial cell attachment and mitochondrial activity, the higher oxidative stress may limit its suitability for extended applications requiring prolonged cell viability and interaction.

Notably, S5 demonstrated enhanced support in co-culture assays, likely attributed to its high density of surface carboxyl groups derived from excess TMA, which may facilitate differential adhesion or other signalling pathways relevant to multicellular interaction. However, its dense crosslinked structure and low porosity impair mechanotransduction and $Ca^{2+}$-signalling, as evidenced by reduced intracellular $Ca^{2+}$-levels. In contrast, S3 exhibited strong performances in modulating mitochondrial membrane potential and cellular oxidative stress, due to its balanced porosity and moderate stiffness. Yet, its lower surface carboxyl density and intermediate mechanical characteristics may not favour sustained multicellular adhesion in co-culture settings. These findings indicate that different formulations preferentially support specific cellular functions, suggesting that hybrid scaffold designs may be needed to integrate multiple performance criteria.

Nevertheless, polyesters S1 (1 : 0.5 PEG : TMA) and S2 (1 : 1 PEG : TMA) demonstrate sufficient biocompatibility, supporting adhesion of HaCaT and F-11 cells. However, their smoother surface morphologies, as observed in AFM and SEM, and low branching percentages (26% for S1 and 40% for S2) result in reduced functional complexity. These limitations may be in accord with fewer neuronal extensions and weaker neuro–keratinocyte interactions. We speculate that the reduced number of functional end groups and inadequate mechanical cues may be provided by these surfaces which hinder their efficacy in facilitating complex tissue interactions.

The distinct cellular behaviours observed across the polyester surfaces can be directly linked to their molecular and surface properties. S5 has a highly crosslinked and branched structure which creates a stable platform that supports robust cell adhesion and communication while mitigating oxidative stress. In contrast, S3's balanced porosity and crosslinking promote cellular growth and mitochondrial activation but may induce oxidative stress over time. S1 and S2, lacking sufficient branching and functional group density, fail to provide the necessary structural and biochemical cues for effective neuro–keratinocyte co-culture.

Thus, polyester S5 emerges as the optimal biomaterial for neuro–epidermal tissue engineering applications, offering a favourable environment for neuro–keratinocyte interactions. Its ability to support neuronal adhesion, keratinocyte alignment, and neurite outgrowth, while minimizing oxidative stress and enhancing mitochondrial function, highlights its potential for applications in nerve repair, wound healing, and burn treatment. S3 offers a viable alternative for applications requiring moderate interaction and short-term cell viability, while S1 and S2 are less suitable for applications necessitating complex neuro–keratinocyte coordination.

## 4. Conclusions

Polyesters synthesized from PEG and TMA in varying stoichiometric ratios (S1–S5) exhibit a direct correlation between structural architecture and biological functionality, highlighting the role of molecular design in biomaterial performance. Controlled stoichiometry and reaction parameters effectively mitigated premature gelation, yielding polyesters with tunable branching and crosslinking.

Among the formulations, S3 (1 : 2 PEG : TMA) displayed optimal branching and microvoid networks (~0.73 μm), facilitating nutrient diffusion and cell adhesion. This architecture enhanced mitochondrial activity, indicated by increased MMP and ROS production, although moderate oxidative stress could limit its suitability for applications requiring sustained low ROS levels. Conversely, the hyperbranched, densely crosslinked structure of S5 (1 : 5 PEG : TMA) exhibited reduced ROS levels and enhanced mitochondrial function, fostering a stable microenvironment conducive to cellular metabolic processes. However, as ROS production is induced by multiple factors, a "direct and linear" relationship of ROS production with surfaces used only is difficult to establish. This architecture supported robust neuro–keratinocyte interactions, demonstrated by neurite extensions across keratinocyte junctions and the formation of tight cellular assemblies.

Intracellular $Ca^{2+}$-dynamics further illustrated the impact of polyester architecture on cellular signaling. S1 and S2 minimally altered $Ca^{2+}$-homeostasis due to their simpler structures, whereas S5 has compact architecture significantly modulated mechanotransduction pathways, enhancing neuro–keratinocyte co-culture outcomes. S5 has the capacity to facilitate synchronized neuronal and keratinocyte activity, which positions it as a candidate for advanced tissue regeneration applications, particularly nerve repair and wound healing.

Future research will involve *in vivo* evaluations to assess long-term biocompatibility, biodegradation profiles, and efficacy in tissue repair models.[54] Incorporating bioactive molecules or growth factors into the polyester matrix may further augment cellular responses. Additionally, optimizing synthesis scalability and reproducibility will be critical for clinical translation. Advanced computational modeling and machine learning approaches could provide insights into the relationship between polyester architecture and cellular dynamics, guiding the design of next-generation biomaterials for complex tissue engineering challenges.[55]

## Author contributions

AM: conceptualization, methodology, formal analysis, investigation, writing – original draft, writing – review & editing; SK: conceptualization, methodology, formal analysis, investigation, writing – original draft, writing – review & editing; SB: formal

analysis, investigation, writing – original Draft, writing – review & editing; LG: conceptualization, methodology, formal analysis, investigation, writing – review & editing, resources, supervision; CG: conceptualization, methodology, formal analysis, investigation, writing – review & editing, resources, supervision; JC: conceptualization, methodology, formal analysis, investigation, writing – review & editing; PG: conceptualization, methodology, formal analysis, investigation, writing – review & editing, resources, supervision; RM: conceptualization, methodology, formal analysis, investigation, writing – review & editing, resources; AB: conceptualization, methodology, formal analysis, investigation, writing – review & editing, resources, supervision.

## Conflicts of interest

All individuals listed as authors qualify as authors and have approved the submitted version. Their work is original and is not under consideration by any other journal. They have permission to reproduce any previously published material.

## Data availability

The authors declare that the data supporting the findings of this study are available within the paper and its SI. Should any raw data files be needed in another format they are available from the corresponding author upon reasonable request.

Supplementary information available: Table S1: nomenclature, stoichiometry, solubilization, and yield percentage of the polymer, and Table S2: detailed characteristic features of polyesters. See DOI: **https://doi.org/10.1039/d5ma00216h**

## References

1 J. A. McGrath, R. A. J. Eady and F. M. Pope, Anatomy and organization of human skin, *Rook's textbook of dermatology*, 2004, vol. 1, pp. 3–2.
2 H. Wang, Z. Xiong and C. Liu, *et al.*, Hyperbranched polymeric scaffolds for tissue engineering, *J. Biomed. Mater. Res., Part A*, 2004, **68**(3), 411–419, DOI: **10.1002/jbm.a.20028**.
3 S. Shetty and S. Gokul, Keratinization and its disorders, *Oman Med. J.*, 2012, **27**(5), 348.
4 J. Uitto, G. Richard and J. A. McGrath, Diseases of epidermal keratins and their linker proteins, *Exp. Cell Res.*, 2007, **313**(10), 1995–2009.
5 P. Chieosilapatham, C. Kiatsurayanon, Y. Umehara, J. V. Trujillo-Paez, G. Peng, H. Yue and F. Niyonsaba, Keratinocytes: innate immune cells in atopic dermatitis, *Clin. Exp. Immunol.*, 2021, **204**(3), 296–309.
6 E. Žagar, M. Žigon and S. Podzimek, Characterization of commercial aliphatic hyperbranched polyesters, *Polymer*, 2006, **47**(1), 166–175.
7 S. Pedrón, C. Peinado, P. Bosch and K. S. Anseth, Synthesis and characterization of degradable bioconjugated hydrogels with hyperbranched multifunctional cross-linkers, *Acta Biomater.*, 2010, **6**(11), 4189–4198.
8 X. Zhou, Y. Chen, L. Cui, Y. Shi and C. Guo, Advances in the pathogenesis of psoriasis: from keratinocyte perspective, *Cell Death Dis.*, 2022, **13**(1), 81.
9 M. Yadav and C. Goswami, TRPV3 mutants causing Olmsted Syndrome induce impaired cell adhesion and nonfunctional lysosomes, *Channels*, 2017, **11**(3), 196–208.
10 T. K. Acharya, S. Kumar, N. Tiwari, A. Ghosh, A. Tiwari, S. Pal and C. Goswami, TRPM8 channel inhibitor-encapsulated hydrogel as a tunable surface for bone tissue engineering, *Sci. Rep.*, 2021, **11**(1), 3730.
11 S. V. Murphy and A. Atala, 3D bioprinting of tissues and organs, *Nat. Biotechnol.*, 2014, **32**(8), 773–785, DOI: **10.1038/nbt.2958**.
12 R. Chakraborty, T. K. Acharya, N. Tiwari, R. K. Majhi, S. Kumar, L. Goswami and C. Goswami, Hydrogel-mediated release of TRPV1 modulators to fine tune osteoclastogenesis, *ACS Omega*, 2022, **7**(11), 9537–9550.
13 S. Kumar, R. K. Majhi, S. Sanyasi, C. Goswami and L. Goswami, Acrylic acid grafted tamarind kernel polysaccharide-based hydrogel for bone tissue engineering in absence of any osteo-inducing factors, *Connect. Tissue Res.*, 2018, **59**(sup1), 111–121, DOI: **10.1080/03008207.2018.1442444**. PMID: 29458266.
14 A. Bandyopadhyay, S. Sengupta and T. Das, *Hyperbranched polymers for biomedical applications*, Springer, Singapore, 2018.
15 D. E. Discher, P. Janmey and Y. Wang, Tissue cells feel and respond to the stiffness of their substrate, *Science*, 2005, **310**(5751), 1139–1143, DOI: **10.1126/science.1116995**.
16 N. Annabi, A. Tamayol and J. A. Uquillas, *et al.*, Hydrogel-based scaffolds for tissue engineering applications, *Adv. Mater.*, 2014, **26**(1), 85–124, DOI: **10.1002/adma.201303233**.
17 Q. P. Pham, U. Sharma and A. G. Mikos, Electrospinning of polymeric nanofibers for tissue engineering applications: A review, *Tissue Eng.*, 2006, **12**(5), 1197–1211, DOI: **10.1089/ten.2006.12.1197**.
18 M. P. Lutolf and J. A. Hubbell, Synthetic biomaterials as instructive extracellular microenvironments for morphogenesis in tissue engineering, *Nat. Biotechnol.*, 2005, **23**(1), 47–55, DOI: **10.1038/nbt1055**.
19 N. A. Peppas and R. Langer, New challenges in biomaterials, *Science*, 1994, **263**(5154), 1715–1720, DOI: **10.1126/science.8134835**.
20 M. W. Tibbitt and K. S. Anseth, Hydrogels as extracellular matrix mimics for 3D cell culture, *Biotechnol. Bioeng.*, 2009, **103**(4), 655–663, DOI: **10.1002/bit.22361**.
21 X. Fu, X. Dong and X. Sun, *et al.*, Muscle stem cell loss and regeneration capacity decline with aging, *Stem Cells Dev.*, 2015, **24**(24), 2748–2758, DOI: **10.1089/scd.2015.0186**.
22 R. R. Rao and J. P. Stegemann, Cell-based approaches to the engineering of vascularized muscle constructs, *Acta Biomater.*, 2013, **9**(9), 8069–8083, DOI: **10.1016/j.actbio.2013.06.043**.
23 M. A. Weber and W. Frueh, The impact of biocompatible scaffolds on muscle regeneration in older adults, *Curr. Opin. Biotechnol*, 2018, **60**, 45–52, DOI: **10.1016/j.copbio.2019.08.012**.

24 B. Geiger, J. P. Spatz and A. D. Bershadsky, Environmental sensing through focal adhesions, *Nat. Rev. Mol. Cell Biol.*, 2009, **10**(1), 21–33, DOI: 10.1038/nrm2593.
25 T. Mammoto and D. E. Ingber, Mechanical control of tissue and organ development, *Development*, 2010, **137**(9), 1407–1420, DOI: 10.1242/dev.024166.
26 J. Zhu and R. E. Marchant, Design properties of hydrogel tissue-engineering scaffolds, *Expert Rev. Med. Devices*, 2011, **8**(5), 607–626, DOI: 10.1586/erd.11.27.
27 B. S. Kim, C. E. Baez and A. Atala, Biomaterials for tissue engineering, *World J. Urol.*, 2000, **18**(1), 2–9, DOI: 10.1007/s003450050013.
28 W. D. Fakhouri, B. T. Phillips and C. J. Koh, Recent advances in PEG hydrogels for biomedical applications, *Mater. Today*, 2015, **18**(4), 211–219, DOI: 10.1016/j.mattod.2014.08.014.
29 R. N. Judson and H. Wackerhage, Cellular mechanisms of muscle repair and regeneration in the elderly, *Nat. Rev. Mol. Cell Biol.*, 2017, **18**(5), 267–278, DOI: 10.1038/nrm.2017.15.
30 K. Ghosal, S. K. Bhattacharyya, V. Mishra and H. Zuilhof, Click Chemistry for Biofunctional Polymers: From Observing to Steering Cell Behavior, *Chem. Rev.*, 2024, **124**(23), 13216–13300.
31 J. D. Hartgerink, E. Beniash and S. I. Stupp, Self-assembly and mineralization of peptide-amphiphile nanofibers, *Science*, 2001, **294**(5547), 1684–1688, DOI: 10.1126/science.1063187.
32 C. Gao, D. Yan and H. Frey, Hyperbranched polymers: From synthesis to applications, *Prog. Polym. Sci.*, 2004, **29**(3), 183–275, DOI: 10.1016/j.progpolymsci.2003.12.002.
33 N. J. Oldham, NMR characterization of polymer materials, *Anal. Bioanal. Chem.*, 2009, **394**(1), 9–20, DOI: 10.1007/s00216-009-2619-6.
34 A. Mukherjee, S. Dutta, R. Sarkar, S. Basak, S. Sengupta, S. Chakraborty and A. Bandyopadhyay, Synthesis and Characterization of Hyperbranched Polyesters from Polyethylene Glycol and Citric Acid: Structural Insights and Antibiotic Resistance Mitigation against Drug-Resistant Bacterial Strains, *New J. Chem.*, 2025, **49**(5), 1883–1898.
35 R. Sarkar, R. Chatterjee, S. Dutta, S. Kumar, S. Kumar, C. Goswami and A. Bandyopadhyay, Cytocompatible Hyperbranched Polyesters Capable of Altering the $Ca^{2+}$ Signaling in Neuronal Cells *In Vitro*, *ACS Appl. Bio Mater.*, 2024, **7**(10), 6682–6695.
36 P. D. Dalton, L. Flynn, M. S. Shoichet and D. J. Mooney, Cell behavior in 3D matrices, *Curr. Opin. Biotechnol*, 2002, **13**(5), 443–455, DOI: 10.1016/S0958-1669(02)00338-8.
37 A. J. Engler, S. Sen, H. L. Sweeney and D. E. Discher, Matrix elasticity directs stem cell lineage specification, *Cell*, 2006, **126**(4), 677–689, DOI: 10.1016/j.cell.2006.06.044.
38 A. Mukherjee, S. Sengupta, B. Singha, R. Chatterjee, S. Chakraborty, A. Singh and A. Bandyopadhyay, Ratiometric synthesis of non-traditional polyesters from poly(ethylene glycol) and trimesic acid tethering bioapplication, *J. Polym. Res.*, 2023, **30**(8), 299.
39 S. Sengupta, S. Kumar, T. Das, L. Goswami, S. Ray and A. Bandyopadhyay, A polyester with hyperbranched architecture as potential nano-grade antibiotics: an *in vitro* study, *Mater. Sci. Eng., C*, 2019, **99**, 1246–1256.
40 K. Wang, K. Amin, Z. An, Z. Cai, H. Chen, H. Chen and B. Z. Tang, Advanced functional polymer materials, *Mater. Chem. Front.*, 2020, **4**(7), 1803–1915.
41 M. A. Beach, U. Nayanathara, Y. Gao, C. Zhang, Y. Xiong, Y. Wang and G. K. Such, Polymeric Nanoparticles for Drug Delivery, *Chem. Rev.*, 2024, **124**(9), 5505–5616.
42 M. Jikei, K. Fujii, G. Yang and M. A. Kakimoto, Synthesis and properties of hyperbranched aromatic polyamide copolymers from AB and AB2 monomers by direct polycondensation, *Macromolecules*, 2000, **33**(17), 6228–6234.
43 R. Q. Li, T. Huang and S. L. Gong, Preparation of high hydroxyl self-emulsifying polyester and compounding with acrylate, *J. Appl. Polym. Sci.*, 2020, **137**(2), 48278.
44 N. G. Ricapito, C. Ghobril, H. Zhang, M. W. Grinstaff and D. Putnam, Synthetic biomaterials from metabolically derived synthons, *Chem. Rev.*, 2016, **116**(4), 2664–2704.
45 J. Avossa, G. Pota, G. Vitiello, A. Macagnano, A. Zanfardino, M. Di Napoli and G. Luciani, Multifunctional mats by antimicrobial nanoparticles decoration for bioinspired smart wound dressing solutions, *Mater. Sci. Eng., C*, 2021, **123**, 111954.
46 S. Shi, H. Zeng, T. Jin, L. Liu, L. Xie, Y. Lin and L. Zhang, Novel hyperbranched resin for wood adhesive: Based on air oxidation and crosslinking copolymerization strategy, *Polym. Test.*, 2023, **126**, 108154.
47 F. Khan, M. Atif, M. Haseen, S. Kamal, M. S. Khan, S. Shahid and S. A. Nami, Synthesis, classification and properties of hydrogels: Their applications in drug delivery and agriculture, *J. Mater. Chem. B*, 2022, **10**(2), 170–203.
48 M. Arkas, M. Vardavoulias, G. Kythreoti and D. A. Giannakoudakis, Dendritic polymers in tissue engineering: Contributions of PAMAM, PPI PEG and PEI to injury restoration and bioactive scaffold evolution, *Pharmaceutics*, 2023, **15**(2), 524.
49 M. Iza, G. Stoianovici, L. Viora, J. L. Grossiord and G. Couarraze, Hydrogels of poly(ethylene glycol): mechanical characterization and release of a model drug, *J. Controlled Release*, 1998, **52**(1–2), 41–51.
50 K. M. Fuller, D. Clay, S. R. Almahdali, A. Paterson, C. M. Barratt, V. Desyatkin and V. O. Rodionov, Arm-first synthesis of hyperbranched-core star polymers via copper-catalyzed azide-alkyne cycloaddition, *Eur. Polym. J.*, 2023, **190**, 111987.
51 W. Chen, X. Shen, Y. Hu, K. Xu, Q. Ran, Y. Yu and K. Cai, Surface functionalization of titanium implants with chitosan-catechol conjugate for suppression of ROS-induced cells damage and improvement of osteogenesis, *Biomaterials*, 2017, **114**, 82–96.
52 D. B. Zorov, M. Juhaszova and S. J. Sollott, Mitochondrial reactive oxygen species (ROS) and ROS-induced ROS release, *Physiol. Rev.*, 2014, **94**(3), 909–950.
53 Z. Tu, Y. Zhong, H. Hu, D. Shao, R. Haag, M. Schirner and K. W. Leong, Design of therapeutic biomaterials to control inflammation, *Nat. Rev. Mater.*, 2022, **7**(7), 557–574.

54 X. Xu, S. Xu, J. Wan, D. Wang, X. Pang, Y. Gao and X. Sun, Disturbing cytoskeleton by engineered nanomaterials for enhanced cancer therapeutics, *Bioact. Mater.*, 2023, **29**, 50–71.

55 P. Dimitriou, Microfluidic construction and operation of artificial cell chassis encapsulating living cells and pharmaceutical compounds towards their controlled interaction, Doctoral dissertation, Cardiff University, 2023.